Meteorol Atmos Phys (2012) 118:65–78
DOI 10.1007/s00703-012-0200-1

ORIGINAL PAPER

Kinetic energy budget of Typhoon Yagi (2006) during its extratropical transition

Yuan Sun · Zhong Zhong · Yuan Wang

Received: 23 October 2011 / Accepted: 9 June 2012 / Published online: 29 June 2012

Abstract A diagnostic energetic analysis is conducted to study the kinetic energy budget during the extratropical transition (ET) of tropical cyclone (TC) Yagi (2006), using high-resolution numerical model output. The results show that the upper-level jet stream makes great contribution to the redevelopment of Yagi. When the Yagi approached to the upper-level jet stream, the horizontal flux of kinetic energy associated with the jet was the major cause of the ET. During the transition of Yagi, the horizontal flux of kinetic energy caused by the change of environmental field related to the TC movement only accounted for about 25 % of the total flux, while the horizontal convergence to Yagi under the action of the jet was the major portion of the total horizontal flux. Moreover, the work of pressure gradient force changed from a source of kinetic energy to a sink in the upper troposphere before and after the ET, however, it acted as a source of kinetic energy in the lower and middle troposphere all the time, and both the vertical and horizontal fluxes of kinetic energy caused by the upper-level jet increased the kinetic energy in the upper troposphere. The sub-grid scale friction and dissipation, which shows their maximum effects in the lower troposphere especially in the atmospheric boundary layer, played major consumption roles against the pressure gradient force. Furthermore, the consumption was almost entirely out-of-phase for the convective transport of kinetic energy in vertical, and inhibited the vertical flux of kinetic energy. In addition, there were significant high-frequency disturbances before and after the ET characterized by out-of-phase kinetic energy changes between upper and lower levels, thus, the vertically integrated kinetic energy budget in the air column could not give a reasonable physical image for TC kinetic energy variation.

Responsible editor: L. Gimeno.

Y. Sun · Z. Zhong (✉)
Institute of Meteorology and Oceanography, PLA University of Science and Technology, No. 60, Shuanglong Road, Nanjing 211101, China
e-mail: zhong_zhong@yeah.net

Y. Wang
Key Laboratory of Mesoscale Severe Weather/Ministry of Education/School of Atmospheric Science, Nanjing University, Nanjing, China

1 Introduction

When a tropical cyclone (TC) moves to a region of prevailing mid-latitude westerlies, its structure will change, in order to adapt to the environmental wind, temperature, and humidity. Such structural change often leads to the transition of a TC into an extratropical cyclone (Harr et al. 2000). The transition process of a TC can lead to a rapid intensification of its strength sometimes, causing enormous damages to marine and coastal facilities when making a landfall (Jones et al. 2003).

There is no commonly accepted definition of extratropical transition (ET). A variety of factors have been assessed by different forecast centers to decide whether or not a TC is undergoing ET (Jones et al. 2003). The ET process of a TC was divided into two stages by Klein et al. (2000), namely, the evolutionary process of TC structure (transformation stage, hereafter TS) and the development process of a TC as an extratropical cyclone (reintensification stage, hereafter RS). The TS was defined to begin with an asymmetric appearance of clouds and, especially, a widespread decrease of deep convection in the western quadrant of the TC, and to complete when the TC has the

characteristics of a baroclinic cyclone and the center of the storm is embedded in cold, descending air. The RS is defined to begin when the transformed storm has achieved its minimum sea level pressure (MSLP) at or after the completion of the transformation, and to conclude at the synoptic time when the reintensified storm has achieved the deepest MSLP before either filling or holding steady in the next analysis.

During the first stage, the movement of a TC is often accelerated and its asymmetric structure becomes more notable. Furthermore, the transition of a TC is often accompanied by the development of a dipole structure in the thermal and vorticity advections, and the maximum intensity of this dipole could be used to determine whether the transformation and reintensification of a TC have occurred or not (Klein et al. 2000). The persistent asymmetric structure at 900–600 hPa was taken as the start of TC transition to extratropical cyclone (Evans and Hart 2003), while the appearance of a cold vortex center was considered as the end of the transition. For the RS after the TS of a TC, the importance of the westerlies was emphasized by DiMego and Bosart (1982), Harr et al. (2000), and Harr and Elsberry (2000). It was considered that the RS was similar to that of Type-B extratropical cyclogenesis (Petterssen and Smebye 1971), namely, downward delivery of kinetic energy leads to the development of lower-level cyclone. Bosart and Lackmann (1995) stated that, in addition to the existence of extratropical cyclone, favorable environmental factors were also beneficial to the reintensification of an extratropical cyclone. Sinclair (1993) showed that the ascending motion caused by equatorial cyclonic vorticity advection of the upper-level jet stream was also beneficial to the development of storm. Through numerical simulations of the reintensification after the ET in the Northwest Pacific, Klein et al. (2000) found that the interaction between the westerlies and a TC was a dynamically complex process, rather than a static one. Upper tropospheric outflow of the transforming storm was confluent with the polar jet, which was well north of the storm. However, the onset of vertical wind shear to the south of the jet "ventilated" the storm by advecting the top of the upper tropospheric warm core downstream, and produced a tilt downstream of isentropic surfaces and contours of potential vorticity, and a vertical motion dipole with maximum ascent (descent) located downshear and downshear-left (upshear and upshear-right). Therefore, an eyewall developed (collapsed) at the side of downshear and downshear-left (upshear and upshear-right), resulting in a TC with an asymmetric structure and extratropical cyclone characteristics. Moreover, the relative position between a TC and a jet stream was also very important to the development of a cyclone (Klein et al. 2000).

The ET of a TC is a highly complex process, during which both dynamic structure and thermal structure of the TC have undergone significant changes. In order to identify the energy sources of TC transition and the causes for its reintensification, analysis of kinetic energy budget of a cyclone is an effective approach. In the late 1970s and early 1980s, the kinetic energy balance equation was used for the analysis on kinetic energy budget of a TC by many researchers. The results showed that the upper-level jet stream played a crucial role in the transition process of a poleward cyclone. However, due to differences in area, case, and the relative position between the jet stream and a cyclone, the relative importance of kinetic energy budget terms is often quite different from one to another (e.g., Kornegay and Viecent 1976; Chien and Smith 1977; Chen et al. 1978).

So far, most studies on the ET process of a TC have been conducted using observational data. In those studies, detailed changes of kinetic energy budget terms in the transition process could not be accurately reflected due to low temporal and spatial resolutions of the observational data. In particular, since the computation of generation terms of kinetic energy is related to ageostrophic motion, both temporal and spatial resolutions of observations need to be sufficiently high. Otherwise, it would be difficult to ensure the accuracy of calculations (Kung 1966).

In this study, the characteristics of kinetic energy budget in the ET and reintensification process of a TC are investigated by taking Yagi (2006) as an example, which was a TC in the Northwest Pacific during September 2006, and by using the high-resolution simulation results before and after Yagi's transition. In Sect. 2, the numerical model and the simulation are described. The analyses on kinetic energy budget during the ET are shown in Sect. 3, followed by the conclusions in Sect. 4.

2 Description of the model and verification of simulation results

2.1 TC case

Yagi was the 14th TC in the western Pacific in 2006, and was generated at 0600 UTC on 17 September at (21.0°N, 157.6°E). It was gradually intensified into a typhoon at 0600 UTC on 19 September, which reached the maximum intensity at 0000 UTC on 22 September with the MSLP of 920 hPa. After that, its intensity began to decrease. The TC propagated northwestward first, followed by a northeastward displacement at 1800 UTC on 22 September with an accelerated movement. Yagi began to experience ET over the ocean to the east of Japan at 0600 UTC on 25 September and redeveloped thereafter (Song et al., 2011).

Figure 1 shows the horizontal distribution of the National Centers for Environmental Prediction (NCEP) Final Analysis (FNL) wind and its vectors at 200 hPa and the track provided by the Regional Specialized Meteorological Center (RSMC) of Japan Meteorological Administration (JMA). It can be seen that the TC center is located southward of the upper-level jet stream.

According to the classification proposed by Harr et al. (2000) and the track of Yagi, Yagi was classified as a storm in the north-northwestward pattern (Fig. 2). In this study, the transition process of Yagi is simulated, and the kinetic energy budget is analyzed.

2.2 Model configuration and initial conditions

The model used in this study is the Weather Research and Forecasting (WRF) model, developed primarily at the National Center for Atmospheric Research (NCAR) with collaborations of different agencies (Skamarock et al. 2008). The new version of the WRFV3.1 is employed with duplicately nested grid systems in the horizontal on Lambert projection and 35 unevenly layers in the vertical. For a better simulation of a TC, the model domains are movable during the integration (with the new vortex position computed every minute). The corresponding grid point spacing for the two domains are 15 and 5 km, respectively, having 245 × 245 and 154 × 154 grid points in $x \times y$ directions, respectively (Fig. 2). The time step for the coarser domain ($D1$) is 30 s, whereas the 1/3 regulation is used for the fine-mesh domain ($D2$). $D2$ is integrating at the same time as $D1$.

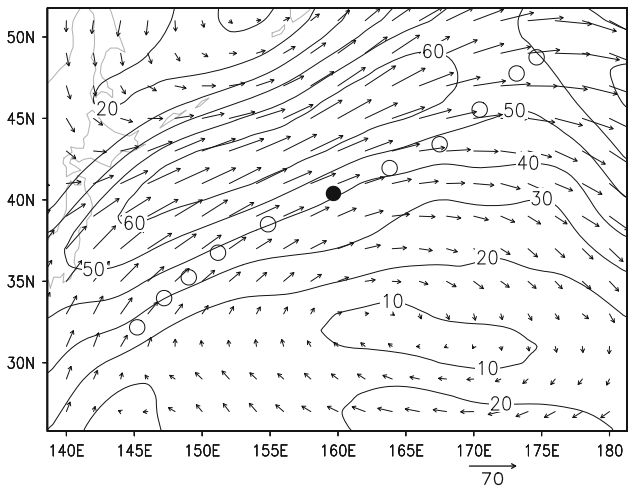

Fig. 1 Wind distribution (vectors; units, m s^{-1}) at 200 hPa using the NCEP/NCAR reanalysis data at 0600 UTC on 25 Sep 2006, and the TC track from the best track data of the RSMC. *Solid circle* the position of TC center at 0600 UTC on 25 Sep 2006, *open circle* the position of TC center at other times

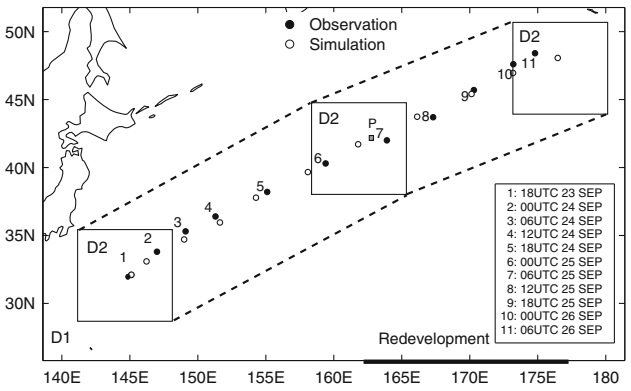

Fig. 2 Design of the two-way nested model domains and track of Yagi's track from the 6-h best track analysis (*filled circles*) and the model (*open circles*)

The related physics processes are calculated with the WRF Single-moment 3-class scheme (Hong et al. 2004) and Lin et al. (1983) scheme for both $D1$ and $D2$. In addition, the Yonsei University non-local-K planetary boundary layer scheme (Hong et al. 2006) is considered for both domains, and the Betts–Miller–Janjic cumulus parameterization scheme (Betts 1986; Betts and Miller 1986; Janjic 1994, 2000) is used in $D1$, whereas no cumulus parameterization scheme is used in $D2$ (Wang 2001; Zhong and Zhang 2006). The longwave and shortwave radiation schemes are taken from the Rapid Radiative Transfer Model (Mlawer et al. 1997) and Dudhia scheme (Dudhia 1989), respectively.

The model integration started at 1800 UTC on 23 September 2006, and ended at 0600 UTC on 26 September 2006, with a total of 60-h integration before and after the ET of Yagi (2006). The model lateral boundary conditions were interpolated from the NCEP FNL dataset with 1° × 1° resolution at 6-h interval, and the forcing of sea-surface temperature (SST) was from the Tropical Rainfall Measuring Mission (TRMM) satellite SST retrieval data with 0.25° × 0.25° resolution once every 24 h. The initial state came from the NCEP first-guess field inserted with a Bogus TC, and the initial position (32.1°N, 145.1°E) was determined according to the best-track data of the RSMC (2006) issued by the JMA (http://www.jma.go.jp/). The model output is at 5-min interval.

2.3 Verification of model results

The best-track data (6-h interval) of the RSMC are used for the verification of track simulation. Figure 2 compares the tracks of Yagi between the observation and simulation, starting from 1800 UTC on 23 September to 0600 UTC on 26 September 2006. It could be seen that the model was able to accurately simulate the track of Yagi, of which the average error of track deviation at 6-h interval was 64 km.

However, the simulated TC translated a little more slowly than the observed from 1200 UTC on 24 September to 0600 UTC on 25 September. Therefore, the simulated TC central positions at 0000 and 0600 UTC on 25 September lagged those of the observed, with the error of more than 100 km at these two moments.

Figure 3 shows the observed and simulated time series of MSLP before and after the transition of Yagi. The average error is about 2.5 hPa, and the maximum error is about 10 hPa. The model is also able to simulate the occurrence time of reintensification of Yagi accurately. The best track reintensification of Yagi occurred between 0000 and 0600 UTC on 25 September, and became notable from 0600 UTC on 25 September; the simulated reintensification of the TC occurred at 0600 UTC on 25 September. However, comparing with the best track, there is a slower (faster) deepening rate in the simulation during (after) the subsequent 6 h.

The evolution of observed and simulated maximum surface wind speed is shown in Fig. 4. It could be seen that the model reproduces well the trend of the maximum wind speed, namely, the gradual decreasing before the ET. Different from that in the tropics, the evolution of maximum wind speed may not match the evolution of MSLP due to the baroclinicity of the TC in the mid-high latitudes, and thus the evolution of maximum wind speed in the RSMC dataset shown in Fig. 4 may be questionable. From the moment 12 h prior to the transition of Yagi, simulated maximum wind speed was higher than that analyzed. The observed maximum wind speed was about 26 m s^{-1}, while the simulated value was 30 m s^{-1} at 0000 UTC on 25 September. Because the maximum wind speed in the RSMC dataset was missing after the transition of Yagi at 0600 UTC on 25 September, a comparison was conducted between the wind field retrieved by QuikSCAT satellite at

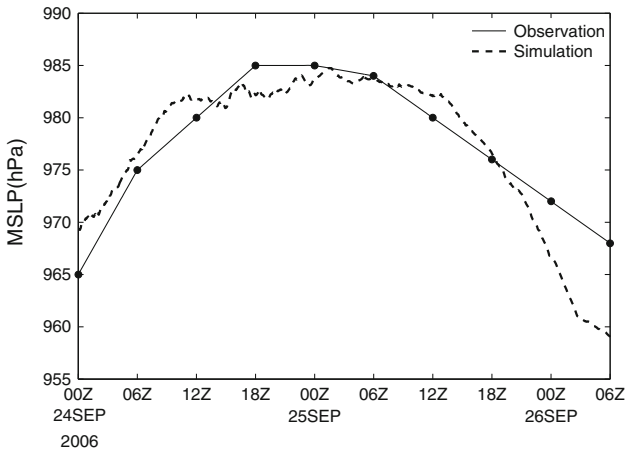

Fig. 3 Observed and simulated temporal variation of MSLP

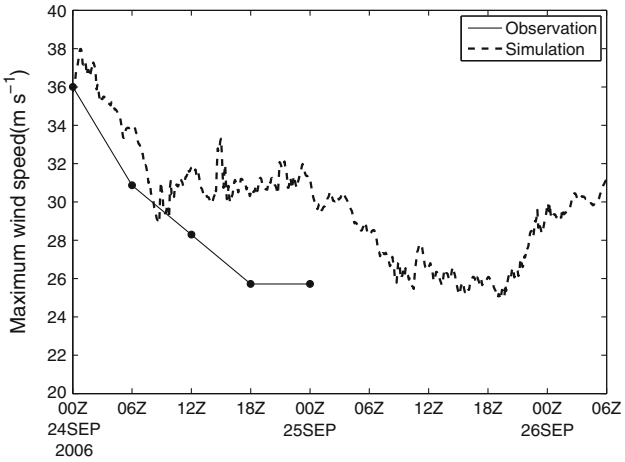

Fig. 4 Observed and simulated temporal variation of the surface maximum wind speed (The data in RSMC dataset was missing after 0000 UTC 25 Sep 2006)

1800 UTC on 25 September and the simulated wind field diagram in *D*1 (Fig. 5).

Figure 5a indicates that the center of Yagi in the wind field diagram retrieved by QuikSCAT was located at 45°N, 172°E and moved with the maximum wind speed of about 32 m s^{-1}, while the simulated center of Yagi was at 44.5°N, 171°E with the maximum wind speed of about 25 m s^{-1}. Meanwhile, both the retrieved and simulated wind fields had the high-wind zone south of the TC center, and both had an area with very low wind speed (<8 m s^{-1}) northwest of the TC center. Furthermore, the distribution of spiral rain bands were similar between the observation and model, with two obvious spiral rain bands in the west and south of the TC center, of which one had a east–west pattern, while the other had a SW–NE pattern. Moreover, the distribution of simulated wind vectors was very similar to that retrieved by the QuikSCAT. Northeasterly and southwesterly winds prevailed west and south of the TC center, respectively, and there was a significant convergence between them.

Following Hart (2003), the cyclone phase space (CPS) method is used to evaluate the ET of a TC. The three parameters of the CPS are:

$$B = \overline{Z_{600\text{hPa}} - Z_{900\text{hPa}}}\big|_{\text{R}} - \overline{Z_{600\text{hPa}} - Z_{900\text{hPa}}}\big|_{\text{L}}, \quad (1)$$

$$V_{\text{T}}^{\text{U}} = -\frac{\partial(Z_{\max} - Z_{\min})}{\partial \ln p}\Big|_{600\text{hPa}}^{300\text{hPa}}, \quad (2)$$

$$V_{\text{T}}^{\text{L}} = -\frac{\partial(Z_{\max} - Z_{\min})}{\partial \ln p}\Big|_{900\text{hPa}}^{600\text{hPa}}, \quad (3)$$

where B measures the degree of lower-tropospheric symmetry, i.e., an area-averaged 900–600 hPa layer thickness, while V_{T}^{U} and V_{T}^{L} are the thermal wind parameters taken as the vertical derivative of height change between two

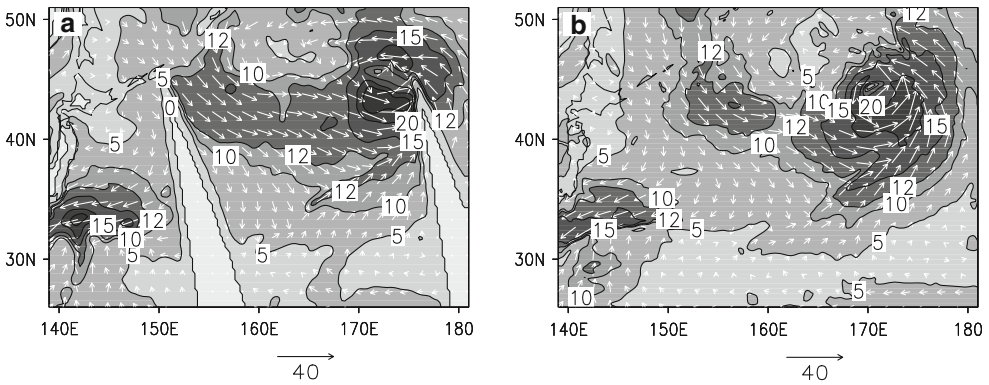

Fig. 5 Comparison of wind (units, m s^{-1}) between **a** QuikSCAT and **b** simulation at 1800 UTC on 25 Sep 2006

isobaric surfaces, i.e., 300–600 and 600–900 hPa for parameters V_T^U and V_T^L, respectively. Z is the geopotential height; subscript R(L) denotes the right (left) semi-square of $D2$ where the area center corresponds with the one of a TC; $Z_{max}(Z_{min})$ refers to the maximum (minimum) value of geopotential height within $D2$; and p represents pressure.

As in Hart (2003), the 10-m threshold for B is used to separate a non-frontal storm from a marginally frontal storm. Negative values of V_T represent a warm-core storm within the layers, while positive values of V_T indicate a cold-core storm within the layers. Furthermore, the start of the ET event is when $|B|$ becomes greater than 10 m; and if V_T^L changes from negative to positive, the ET completes. Note that V_T^U was not used in Hart's ET study (Hart 2003), but was proposed in his paper.

Figure 6 shows the variation of B, V_T^L and V_T^U in the CPS as a function of transit time. A significant feature is that the times for B, V_T^L and V_T^U exceeding their thresholds are not the same, although all of them can be used to distinguish a cyclone undergoing ET from a non-transformed one. Hart (2003) stated that the start of ET was determined by $|B| > 10$ m, while $V_T^L > 0$ could indicate the end of TS of the ET. This implies that V_T^L changes after B. The composite temporal variations of these two parameters agree with this conclusion: $|B|$ surpassed 10 m at 0000 UTC on 25 September, while $V_T^L > 0$ occurred at 0600 UTC on 25 September. Song et al. (2011) utilized the CPS method to evaluate the ET of a TC over the western North Pacific, and indicated that the start of the ET of Yagi was about 0600 UTC on 25 September, which was about 6 h after the start in ours (indentified by $|B|$ firstly surpasses 10 m). For the other parameter, V_T^U transformed from negative to positive in the first place (Hart 2003; Song et al. 2011). This occurred at 0600 UTC on 24 September, about one day before the completion of the transformation, and about 18 h prior to the start of the ET. Moreover, Fig. 6 also shows that the transition from warm core to cold core occurred first in the upper troposphere and then spread down to lower layers. Therefore, in this study, the simulated TS of Yagi started at 0000 UTC on 25 September, and ended at 0600 UTC on 25 September.

Figure 7 shows the horizontal distribution of model-simulated hydrometeors, vector wind, and equivalent potential temperatures at 850 hPa. According to the conceptual model of Klein et al. (2000), a TC translates poleward at the end of its TS (0600 UTC on 25 September for Yagi) with the outer circulation of the TC impinging on a pre-existing baroclinic mid-latitude westerlies (Fig. 7a, b). As the interaction with the baroclinic zone begins, colder and drier environmental equatorward flow appears to the west of the TC, which makes deep convection and reduces hydrometeors in the western quadrant of the TC, and a dry slot forms in the southwestern quadrant with reduced deep convection. Meanwhile, environmental poleward flow to the east of the TC advects warm moist air into the eastern quadrant of the TC, which maintains the deep convection in the quadrant. Then, this environmental poleward flow turns cyclonically and interacts with the pre-existing baroclinic zone to produce an ascent over the titled isentropic surfaces (Fig. 7b). Thus, the eyewall gradually collapses in the western and southern quadrants, and gives an asymmetric appearance. Moreover, the isentropic surfaces title from southwest toward northeast, and are condensed in the northern quadrant of the TC where a vigorous warm frontogenesis has commenced, leading to a gradual increase of the baroclinic energy in the TC. At 1800 UTC on 25 September, the TS has completed and the RS has lasted for 12 h. Also due to the impact of the western colder air and eastern warm air, the convection is suppressed in the western and southern quadrants, but is well developed in the eastern and northern quadrants (Fig. 7c). The isentropic surfaces further tilt and the warm frontogenesis further develops in the northern quadrant of the TC (Fig. 7d), leading to a further development of

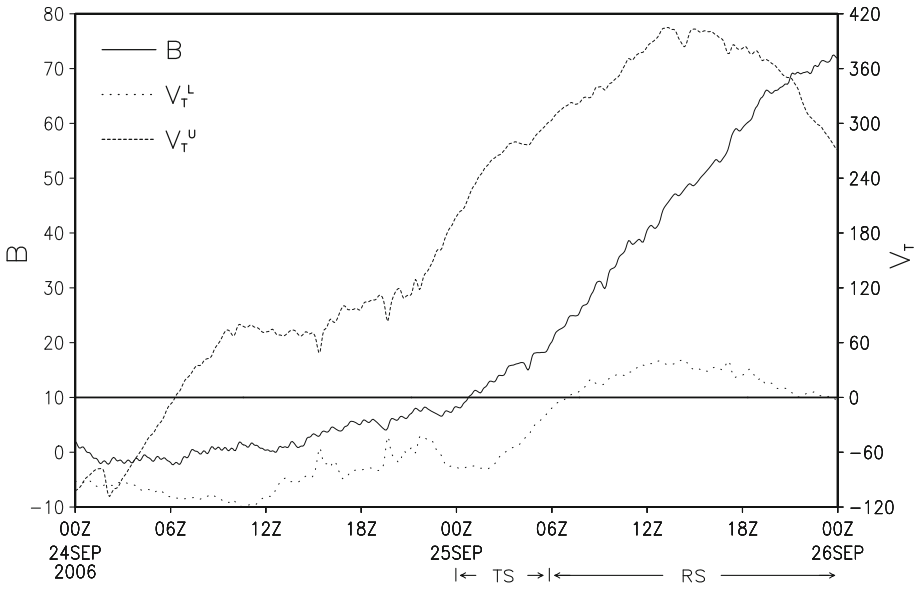

Fig. 6 The temporal evolution of B, V_T^L and V_T^U in the CPS as function of transit time

baroclinic energy in the TC. Therefore, consistent with the conceptual model of Klein et al. (2000), the model results reflect the characteristics of the TS and RS.

In summary, through the analyses and verifications of the evolution of simulated Yagi track, MSLP, and maximum surface wind speed, and of the wind distribution and structure characteristics, it is clear that the evolutionary characteristics of the track, intensity and structure of Yagi before and after the transition are all well reproduced by the WRF forced by the SST retrieved from the TRMM Microware Imager (TMI).

3 Kinetic energy budget

3.1 Kinetic energy equation

Because Yagi is a fast moving weather system, the kinetic energy equation in the Lagrangian coordinate is used in the study, following Kornegay and Viecent (1976).

$$\frac{\delta K}{\delta t}=\frac{1}{gA}\left\{\int_0^{p_0}\int_A -\vec{V}\cdot\nabla\phi\,\mathrm{d}\sigma\mathrm{d}p+\int_0^{p_0}\int_A -\nabla\cdot[(\vec{V}-\vec{W})k]\mathrm{d}\sigma\mathrm{d}p+\int_0^{p_0}\int_A -\frac{\partial k\omega}{\partial p}\mathrm{d}\sigma\mathrm{d}p\right\}+R \tag{4}$$

DK G NHF NVF R

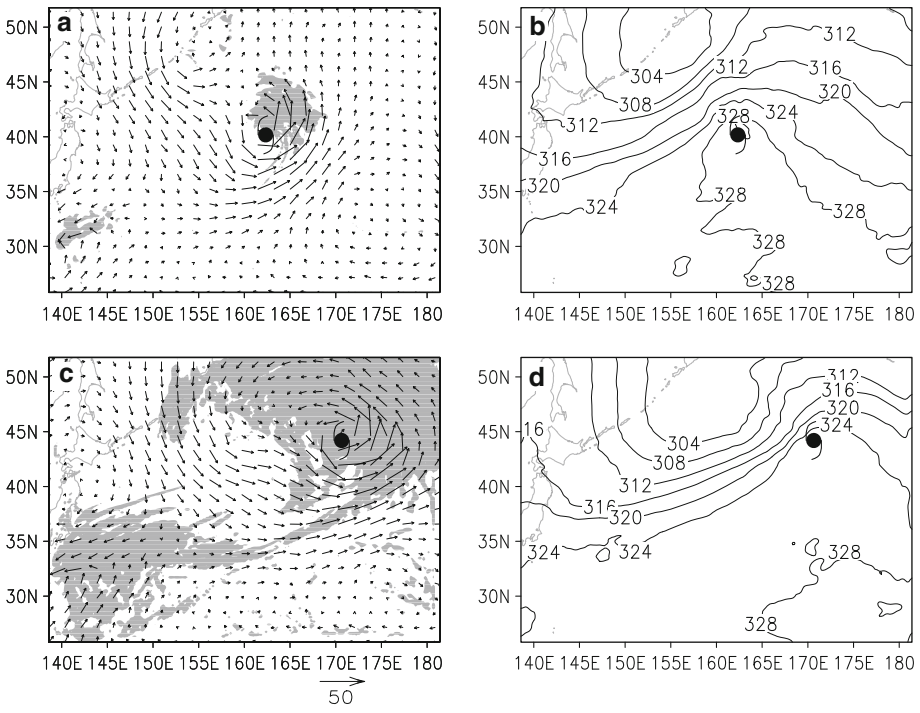

Fig. 7 **a** A top view of the model-simulated hydrometeors (*shaded*), determined by the 0.01 g kg^{-1} surface for cloud water, rain water, ice, snow, and graupel at 0600 UTC on 25 Sep 2006, and wind vector at 850 hPa; **b** equivalent potential temperature (2-K interval) at 850 hPa. **c** and **d** are the same as **a** and **b**, except for 1800 UTC on 25 Sep 2006

$$\underbrace{\int_0^{P_0}\int_A -\nabla\cdot[(\vec{V}-\vec{W})k]\mathrm{d}\sigma\mathrm{d}p}_{\text{NHF}} = \underbrace{\int_0^{P_0}\int_A -\nabla\cdot(\vec{V}\cdot k)\mathrm{d}\sigma\mathrm{d}p}_{\text{NHF1}} + \underbrace{\int_0^{P_0}\int_A \vec{W}\cdot\nabla k\mathrm{d}\sigma\mathrm{d}p}_{\text{NHF2}} \quad (5)$$

In Eq. (4), $\frac{\delta}{\delta t} = \frac{\partial}{\partial t} + \vec{W}\cdot\nabla$, $\vec{W}$ indicates the translation speed of the TC, k is the kinetic energy per unit mass of air parcel, $K = \frac{1}{gA}\int_0^{p_0}\int_A k\mathrm{d}\sigma\mathrm{d}p$ is the vertical integration of kinetic energy per unit area of the air column, DK is the rate of change term of kinetic energy, and G is the generation term of kinetic energy. NHF indicates the horizontal flux divergence term of kinetic energy, composed of the part (NHF1) that does not consider TC movement and the part (NHF2) caused by the TC movement. NVF indicates the vertical flux divergence term of kinetic energy, and R is the residual term (including frictional dissipation, sub-grid scale effect, calculation error, etc.). In the calculation, A is a square with the TC at the center and each side's length is 500 km in the fine-mesh Domain $D2$, which moves with the TC at the same speed of $\vec{W}$. P_0 represents the sea-surface pressure, and the time interval δt is 5 min. In order to ensure the continuity and gradual transition of TC central position together with its translation speed and to ensure no jump due to grid spacing, cubic spline interpolation on TC central latitude and longitude with 2-h time interval was carried out every 5 min; and then the simulation output of the corresponding time is interpolated and calculated at each grid inside the area of 500 × 500 km with 5-km spatial resolution, where the area center corresponds with the relocated center of the TC.

3.2 Characteristics of kinetic energy budget

The simulation results from 1800 UTC on 24 September to 1800 UTC on 25 September, 2006 are used herein for studying the kinetic energy budget during the ET of Yagi. The temporal evolution of kinetic energy and its budget terms of vertical integration over the entire air column within Area A (P_0 is up to 100 hPa) is represented in Fig. 8. Before and after the ET of Yagi, the total kinetic energy (K) of TC increased gradually (to be doubled in 24 h), and it showed the greatest increase in speed in a few hours after the transition. Notable high-frequency disturbances existed in the change rate of kinetic energy (DK). The moving average of DK during the investigating period was positive, and reached the maximum a few hours after the transition of Yagi. The generation of kinetic energy (G), before and after the transition of Yagi, made different contributions to the kinetic energy. G was positive before 1030 UTC on 25 September, indicating that the strongest source of kinetic energy was the available potential energy converted into kinetic energy by pressure gradient force. However, after the TS, G decreased gradually to a negative value and became a sink of kinetic energy. In the studies on the Mediterranean cyclone conducted by Wahab and Basset (2000), it was also found that G could become not only a source of kinetic energy due to positive work of flow crossing the isobaric line to low-pressure area (especially at the weakening stage of a TC) but also a sink of kinetic energy due to negative work of flow crossing the isobaric line to high-pressure area, and it could even become the strongest sink of kinetic energy (especially at the RS of a TC). Similar to the results in Wahab and Basset (2000), the simulation results in this study indicates that G could become not only a source but also a sink of the kinetic energy in the whole transformation and reintensification stages of Yagi, and it is the transition that changes the role and effect of G as a source or a sink of kinetic energy. Horizontal flux divergence (NHF) reflects the kinetic energy exchange between the air in the study area and the surrounding atmosphere, which can be considered as an external source or sink of kinetic energy and its evolution is basically opposite to G. It was negative before the start of RS of Yagi at 0600 UTC on 25 September, but after that time it became even the most important source of kinetic energy. The integrated vertical flux divergence (NVF) in the air column is smaller than any other term in the kinetic energy equation by at least one order of magnitude, similar to the results of Harr et al. (2000) and Wahab and Basset (2000). Residual (R) was basically a weak source of kinetic energy before and after the transition of Yagi. It was negative only in a small number of moments, but its average value during the entire study period was positive, indicating that the kinetic energy was generated by combined effect of sub-grid scale and friction effects. At certain moments, when the conversion of kinetic energy in a sub-grid scale to that in the grid scale can offset the frictional dissipation effect with a residue remained, R could be positive as the source of kinetic energy (Haimberger 1998). As indicated in the analyses of kinetic energy budget on Hurricane Camille (1969) conducted by Chien and Smith (1977) and on the Mediterranean cyclone obtained by Wahab and Basset (2000), due to sub-grid scale effect the residual error term became the most vital source of kinetic energy at the stages of the transformation and reintensification of the TC, and this term had certain correlation with the change rate of kinetic energy (DK).

Residual term R was estimated using Eq. (4). Because the temporal variations of G, NHF, and NVF do not have high-frequency signals, the high-frequency oscillation characteristics of R is highly consistent with that of DK, with the correlation coefficient of 0.88. This is consistent with the findings of Moeng et al. (2004), which showed that turbulent kinetic energy, surface friction velocity, and

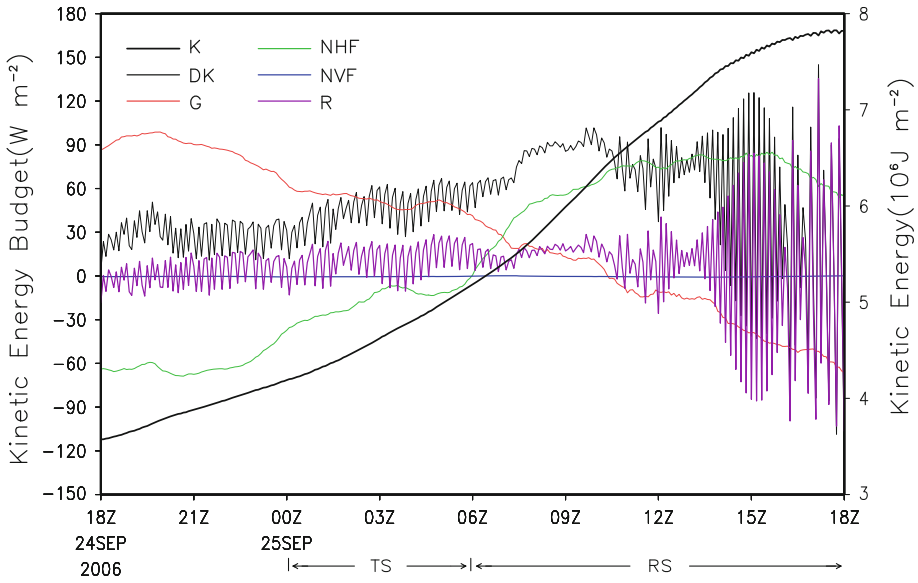

Fig. 8 Temporal evolution of kinetic energy (units, 10^6 J m^{-2}) and its budget terms (units, W m^{-2})

velocity variances were sensitive to sub-gird horizontal diffusion in the model. Therefore, *R* could be taken as one of the causes for generating disturbances in DK. From the evolution characteristics of vertically integrated *R*, we can see that the amplitude of *R* affected the transition of Yagi. The disturbances in *R* were notable before the transition, but was significantly weakened during the transition. However, with the development of baroclinic energy after the transition (after 1200 UTC on 25 September), the disturbances in *R* redeveloped quickly with an intensity much larger than that before the transition (Fig. 8). And from the evolution of vertical distribution of *R*, we can see the effect of *R* varied as a source or a sink of kinetic energy, before and after the transition (discussed in Sect. 3.3), respectively. Moreover, the same significant high-frequency disturbances also existed in the change term of maximum wind speed of Yagi over time (not shown). Therefore, the study on such high-frequency disturbances may have some significance for revealing the mechanism of TC development.

Figure 9 shows the temporary evolution of NHF decomposed into NHF1 without consideration of TC movement and NHF2 caused by TC movement based on Eq. (5). The evolution of NHF1, as the main part (about 75 %) of NHF, is relatively gentle over time. There is a high negative correlation between the evolution of NHF1 and that of *G*, with the correlation coefficient of −0.99. In addition, the conversion of NHF1 from being a sink to being a source of kinetic energy occurred at the commencement of the RS, indicating that the conversion process from kinetic energy (potential energy) to potential energy (kinetic energy) during the RS was closely related to input (output) process with external kinetic energy. That is to say, when the external kinetic energy was added to the TC, the kinetic energy of TC would be converted to potential energy; when the kinetic energy was taken out of the TC, the available potential energy of TC would be converted to kinetic energy. It could also be found in Fig. 9 that the evolution of NHF2 is different from that of NHF1. After the completion of the TS (at about 0600 UTC on 25 September), NHF2 changed slowly. However, after 1200 UTC on 25 September, NHF2 decreased rapidly and became a sink of kinetic energy. Moreover, NHF2 was significantly smaller than NHF1 and could be regarded as a secondary part (about 25 %) of NHF, which partially offset the effect of NHF1 as a kinetic energy source.

From Fig. 8, one can estimate that the period of quasi-periodic disturbances in DK and *R* was about 10–20 min before and after the transition, and the amplitude of such disturbances increased rapidly during the RS. Since the TC was a rapidly moving system, the area of kinetic energy analysis moved with the TC. One may ask whether or not the high-frequency disturbances of DK in kinetic energy equation were due to false signals caused by the movement of the computational domain in this study. Therefore, we now go for an in-depth analysis with the study period from 0000 UTC on 24 September to 1800 UTC on 25 September using the fixed area *P* in Yagi's path of *D*1 (Fig. 10). The fixed area is also shown in Fig. 2 (a shaded area marked by *P*), and is set as a square with the side length of 30 km. The area with maximum wind of Yagi crossed Area *P* at about 0600 UTC on 25 September.

Next, the periodic characteristics of main disturbances in the kinetic energy equation and the sources of such high-frequency disturbances are analyzed. The evolution of DK_P (the rate of change of kinetic energy vertically integrated in the fixed area *P*) and its Morlet wavelet power spectrum are represented in Fig. 10. As expected, quasi-periodic disturbances also existed in DK_P (Fig. 10a). When the maximum

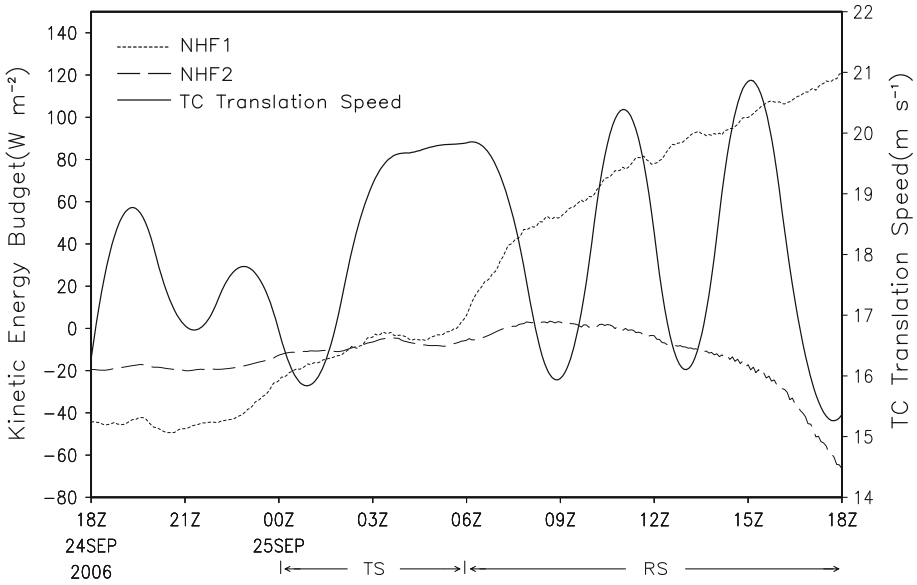

Fig. 9 Temporal evolutions of horizontal flux of kinetic energy that ignores the factor of TC movement (NHF1) and that only considers the TC movement (NHF2), in W m^{-2}, and the moving speed (units, m s^{-1}) of the TC center

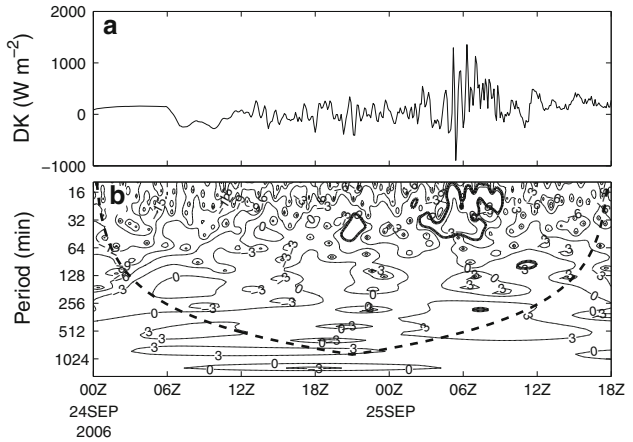

Fig. 10 Temporal evolution **a** and the wavelet power spectrum **b** of rate of change of kinetic energy (DK) in the fixed area of *D*1

wind of Yagi was far from Area *P* (before 1800 UTC on 24 September and after 1200 UTC on 25 September), the variation amplitude of DK_P evolution was nearly negligible over time. However, when the maximum wind of Yagi was adjacent to Area *P* (from 0300 UTC on 25 September to 0900 UTC on 25 September), the variation amplitude of DK_P evolution was extremely large over time, hinting significant disturbances were present around the maximum wind of Yagi. It could be clearly seen in Fig. 10b that the period of 15–30 min is significant at the 95 % level, basically the same as the disturbance period of DK in the above-mentioned moving area *A*. Therefore, the DK disturbances in the moving area *A* were not caused by the movement of the study area *A*, but a true feature of the TC. Such disturbances were most significant in the region of maximum TC wind, and mainly caused by sub-grid scale effect and frictional dissipation effect. It is likely that the presence of the high-frequency disturbances were related to the interaction between the upper-level jet stream and TC circulation, but the mechanism at work needs to be investigated more carefully in future.

3.3 Evolution of vertical distribution of kinetic energy budget terms

Height–time cross sections (Fig. 11) are prepared, in order to study vertical distributions of various kinetic energy budget terms during the transition. As is shown, a huge zone of the upper-level jet stream existed in the upper troposphere (from 300 to 100 hPa; Fig. 1) during the transition and played a key role in the entire transition process of Yagi. When Yagi was adjacent to the upper-level jet stream, the kinetic energy in the upper troposphere increased rapidly. After the transition, Yagi was away from the jet stream but still within the impact zone of the jet stream, the kinetic energy in the upper troposphere continued to increase, but more slowly. The evolution of distribution of kinetic energy in the middle and lower troposphere was significantly slowed down (Fig. 11a). Combining Fig. 11a with Fig. 11b, one could see that the evolution of kinetic energy was significantly different, and it is even opposite for the levels above 500 hPa and the levels below 500 hPa. In the upper troposphere, DK was mainly positive with an average of 4.27 W m^{-2} above 500 hPa, and *K* increased gradually. However, in the lower and middle troposphere, DK was mainly negative with an average of −5.70 W m^{-2} below 500 hPa, and *K* decreased gradually. There were out-of-phase disturbances between upper and lower levels. In other words, the faster (more slowly) the kinetic energy increased in the upper levels, the faster (more slowly) the kinetic energy decreased in the

lower levels; and the period of the disturbances is also about 15–30 min. Thereby, it could be inferred that the high-frequency disturbances of DK may be related to the impact of gravity waves, the frequency for which is similar to that in DK, though this conclusion needs to be verified in future work. The decrease in amplitude of DK disturbances in the transition of Yagi (Fig. 8) was caused by the out-of-phase change of kinetic energy between upper and lower levels. In fact, DK disturbances in the transition were most notable during the study period, especially in the upper troposphere. During the transition period (from 0000 to 1200 UTC on 25 September), the correlation coefficient was −0.91 in evolution of DK between the levels above 500 hPa and the levels below 500 hPa. However, the correlation coefficient was only 0.04 during the entire simulation period (from 1800 UTC on 23 September to 0600 UTC on 26 September). It implies that under the action of the upper-level jet stream during the transition, the changing trends of kinetic energy were opposite between the upper and lower troposphere. The lower-level kinetic energy decreased gradually, while the upper-level kinetic energy increased continuously under the action of the upper-level jet stream; and this out-of-phase change only existed in the transition period.

Figure 11c indicates that the change in the generation term of kinetic energy, G, from a source to a sink of kinetic energy (Fig. 8) is mainly due to the intensification of G as a kinetic energy sink in the middle troposphere, and due to the weakening of G as a kinetic energy source in the lower and upper troposphere during the period before the transition. After the transition, the effect of G as a sink of kinetic energy became more and more notable; and during the RS under the action of the upper-level jet stream, G became a vigorous sink of kinetic energy in the whole middle and upper troposphere, with a maximum center at about 300 hPa. The conclusions from a case study of North American cyclone influenced by the upper-level jet stream by Chen et al. (1978) also indicated that G was a main source of kinetic energy before the transition, but decreased gradually over time after the transition, and became a sink of kinetic energy with a maximum negative center in the middle and upper troposphere (500–200 hPa). Subsequently, negative work was done by pressure gradient force to convert kinetic energy into potential energy. Before and after the transition, the maximum center of G as a source of kinetic energy was in the atmospheric boundary layer, but following the transition process over time, G in the atmospheric boundary layer decreased gradually and then increased slightly after the transition.

The height–time distribution (Fig. 11d) of horizontal flux of kinetic energy, NHF, has a close relationship with the upper-level jet stream. NHF was mainly distributed at the level of the upper-level jet stream, where the position of maximum center of NHF was slightly lower than that of the center of the upper-level jet stream (Fig. 11a). With the approach of the upper-level jet stream and the development of transition process, NHF in the upper troposphere developed rapidly, and became, in replacement of G, the most important source of kinetic energy after the transition. However, with the moving away from the upper-level jet stream, NHF decreased gradually. Therefore, the horizontal flux of kinetic energy was from the horizontal convergence to Yagi under the action of the jet stream.

Figure 11e shows that vertical flux of kinetic energy, NVF, always had a significant positive and negative alternating distribution in the vertical direction. It was positive in the levels below 700 hPa and at 200–100 hPa, while it was negative in the levels at 700–400 hPa and above 200 hPa. Therefore, it indicates that the vertical transfer of kinetic energy was downward (Fig. 11e), which is the development characteristics of Type-B cyclone (Petterssen and Smebye 1971; DiMego and Bosart 1982; Harr and Elsberry 2000; Harr et al. 2000). However, following the transformation and reintensification of Yagi, the downward transfer of kinetic energy decreased gradually over time in the middle troposphere, and the upward transfer of kinetic energy increased in the upper troposphere under the action of the high-level jet stream, which led to a gradual increase in kinetic energy to the upper troposphere. Therefore, to a large extent, the RS of Yagi showed a rapid growth of kinetic energy in the upper troposphere (Fig. 11a). It can be seen from comparing NHF (Fig. 11d) with NVF (Fig. 11e) under the action of the upper-level jet stream that the main contribution of the kinetic energy flux to Yagi was NHF, and that both NHF and NVF had the same contribution to the growth of kinetic energy in the upper troposphere.

It is found that there was an out-of-phase time–space distribution between R and NVF. Before and after the transition, R was a powerful source of kinetic energy in the middle troposphere (700–400 hPa) and top troposphere (above 200 hPa) (Fig. 11f), which is similar to the results by Wahab and Basset (2000), while R was the most powerful sink of kinetic energy in the upper troposphere (400–200 hPa) and lower troposphere (below 700 hPa). It indicates that at the levels where kinetic energy increased (decreased) through vertical transport of kinetic energy, the combined effect of friction and sub-grid scale was a sink (source) of kinetic energy. That is to say, the combination of friction and sub-grid scale acted to inhibit the change of kinetic energy. In the area of losing (gaining) kinetic energy, R acted to increase (decrease) the kinetic energy. Moreover, it can be seen on the height–time cross sections of various kinetic energy budget terms that only R showed significant characteristics of high-frequency disturbances (Fig. 11f).

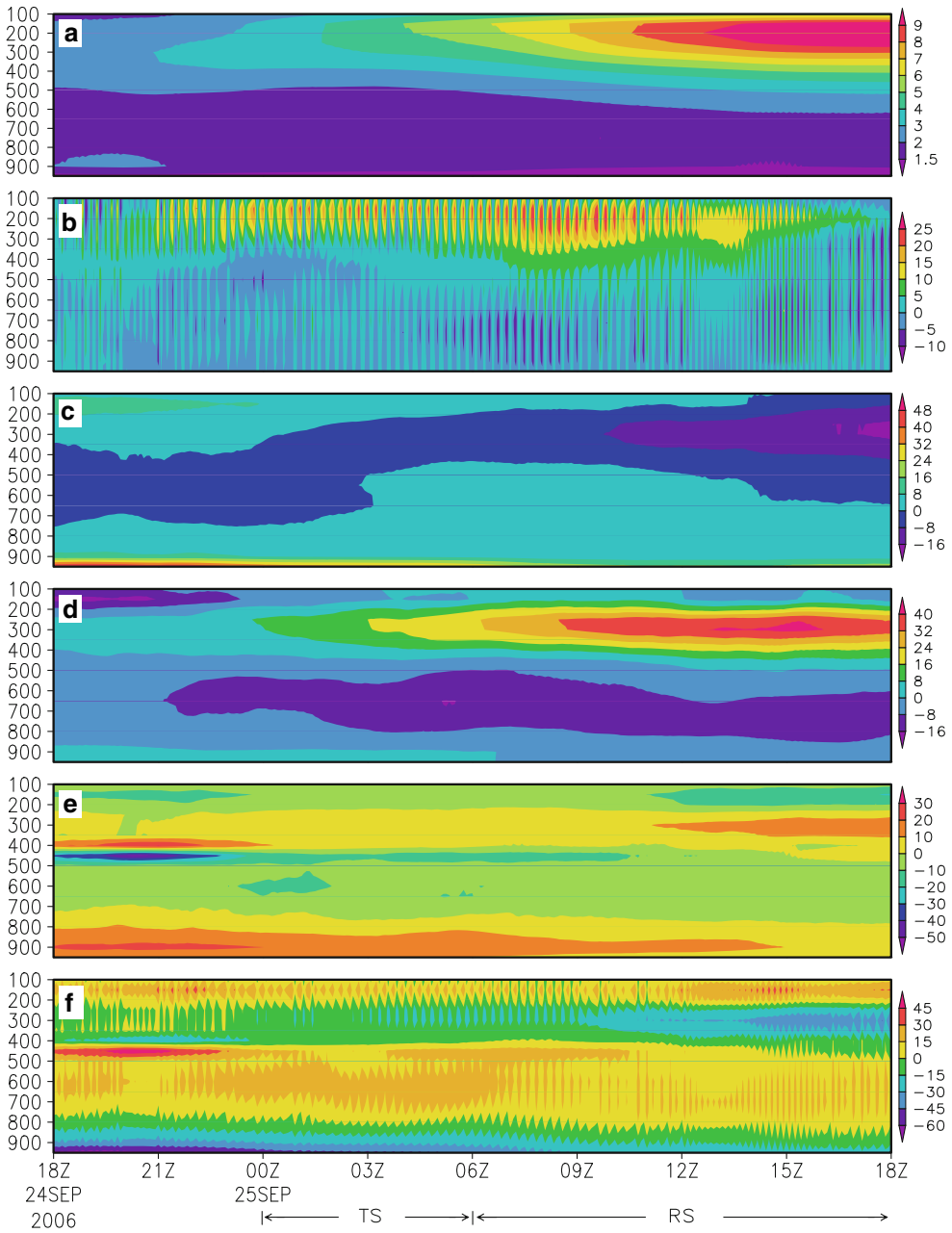

Fig. 11 Height–time sections of kinetic energy (units, 10^5 J m^{-2}) and its budget terms (units, W m^{-2}): **a** kinetic energy (K), **b** rate of change of kinetic energy (DK), **c** generation of kinetic energy (G), **d** horizontal flux of kinetic energy (NHF), **e** vertical flux of kinetic energy (NVF), and **f** the residual (R)

The vertical distribution of NHF shows negligible disturbances over time, and the variation has opposite signs between the upper and lower troposphere (Fig. 11d). In order to identify the cause for these features, NHF is decomposed into NHF1 without consideration of the TC movement (Fig. 12a) and NHF2 related to the TC movement (Fig. 12b). It is revealed that the evolution of vertical distribution of NHF1 is rather smooth, and its spatial distribution is similar to that of NHF; therefore NHF1 could be considered as a major part of NHF. It was pointed out earlier that during the transition period there was an extremely significant negative correlation between G and NHF1 after the vertical integration. Comparing Figs. 11c and 12a, one can see that during the transition period (from 0000 to 1200 UTC on 25 September) both G and NHF1 were present with a line of demarcation at 500 hPa, and the correlation between G and NHF1 was significantly different above and below the line. A positive correlation mainly existed below the line with a correlation coefficient of 0.49. The reason for this correlation is that in the lower troposphere the TC center was the low-pressure center with convergent wind. Positive work was done by an inflow crossing isobaric lines toward the low-pressure center to convert available potential energy into kinetic energy, thus making G, the generation term of kinetic energy, positive. Meanwhile, due to the convergent wind field, the external

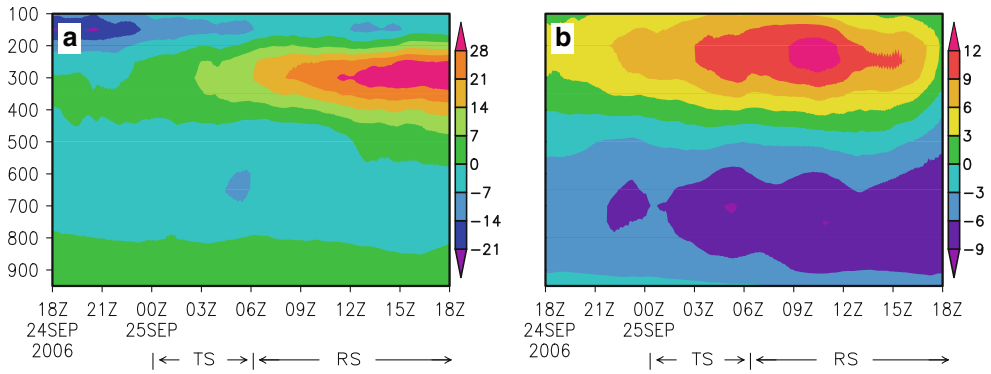

Fig. 12 Height–time sections of horizontal flux of kinetic energy that ignores the factor of the movement of TC (NHF1) (**a**) and that only considers the factor of the movement of TC (NHF2) (**b**) in W m^{-2}

kinetic energy was added to the TC under the action of inflow, leading to positive NHF1 and a significant positive correlation between *G* and NHF1. However, there is an extremely significant negative correlation between *G* and NHF1 above the line, with a correlation coefficient up to −0.93. This is because the TC center was a high-pressure center in the upper troposphere, where the kinetic energy of external jet stream was added to the TC under the action of the upper-level jet stream, leading to positive NHF1 and a convergent wind field. In addition, negative work was done by a flow crossing isobaric lines toward the high-pressure center, leading to negative *G* and significantly negative correlation between *G* and NHF1. Furthermore, by comparing with Fig. 11e, it is found that there was a positive correlation between NHF1 and NVF, which indicates that the horizontal and vertical fluxes of kinetic energy played the same role in changing kinetic energy. Similar to NHF, there was also a line of demarcation at 500 hPa on the height–time cross section of NHF2, with positive NHF2 below the line and negative NHF2 above the line. Comparing Figs. 11b and 12b, one can see that there was a positive correlation between NHF2 and DK. Thereby, the horizontal flux of kinetic energy caused by the change of environment (NHF2) was related to the transition of Yagi.

Similar to DK, there were significant disturbances in the evolution of the vertical distribution of *R*. The disturbances had a significant positive correlation with that of DK; the correlation coefficients with DK disturbances at each height from 950 to 100 hPa at an interval of 50 hPa (approximated by the time-series value at each height minus the average time-series value at the same height) are 0.11, 0.41, 0.56, 0.66, 0.76, 0.80, 0.74, 0.67, 0.60, 0.67, 0.15, 0.47, 0.32, 0.24, 0.41, 0.68, 0.57, and 0.66, respectively, with an average coefficient of 0.57. And the most significant correlation existed at the level of 700 hPa, with a correlation coefficient of 0.80; in contrast, a negligible correlation existed in the boundary layer of troposphere, with a correlation coefficient of 0.11 only. Because the friction effect was much larger than the sub-grid scale effect in the boundary layer, the correlation between *R* and DK was not apt to be caused by friction effect but sub-grid scale effect. In addition, combing Fig. 11e and 11f, one can see that there was a significant negative correlation of time–space distribution between *R* and NVF, and the average coefficient was up to −0.70 at each height. This might be because the vertical flux divergence term had a larger positive value (i.e., the input kinetic energy in the vertical direction), often corresponding to a strong wind shear with a great frictional dissipation effect and leading to a negative residual error term. On the contrary, the vertical flux divergence term had a large negative value (i.e., the output kinetic energy in the vertical direction), often corresponding to a strong sub-grid scale effect and leading to a positive residual error term. In the meantime, there were out-of-phase changes between upper and lower levels in terms of high-frequency disturbances of DK, and the disturbances were mainly around the radius of maximum wind. Therefore, we speculate that such high-frequency disturbances might be closely related to convection through certain mechanism (e.g., gravity waves) and have influence on the evolution of TC maximum wind speed (high-frequency disturbances also existed in the time change term of TC maximum wind speed; not shown).

4 Conclusions

The non-hydrostatic meso-scale model, WRFV3.1, is used to simulate Yagi (2006) in this paper. The simulation has high temporal and spatial resolution for the transition of Yagi over the ocean to the east of Japan. The model results are used for an analysis on kinetic energy budget related to the transformation and reintensification of Yagi. The following conclusions are obtained.

Before the transition of Yagi, due to the effect of an inflow crossing the isobaric lines in the boundary layer, the

positive work, which was done by pressure gradient force to convert available potential energy into kinetic energy, was the most significant source of kinetic energy. After the ET, this positive work decreased gradually in the upper troposphere, and pressure gradient force resulted in negative work and became a sink of kinetic energy after the transition. Horizontal flux of kinetic energy was closely related to the upper-level jet stream, and was the main cause of the ET when approaching the upper-level jet stream. However, with the leaving from the upper-level jet stream, the horizontal flux of kinetic energy decreased gradually. For the term of the horizontal flux, the horizontal flux of kinetic energy caused by the change of environmental field related to the TC movement only accounted for about 25 % of the total flux, while the horizontal convergence to Yagi under the action of the jet stream became the main form of the total horizontal flux. Moreover, after the ET, the latter partially offset the effect of the former as a kinetic energy source. Because of a significant transfer of kinetic energy to the lower levels in the vertical direction, Yagi had significant characteristics of Type-B cyclone during the transition. The effect of friction in the boundary layer made the residual error term of kinetic energy equation a major sink of kinetic energy, and played a role of consuming the positive work done by pressure gradient force and kinetic energy transported by vertical flux.

Analysis of the high-resolution model output shows that there were significant high-frequency disturbances in the evolution of kinetic energy change, DK, with a period of 10–20 min. The high-frequency disturbances were related to the sub-grid scale and friction effects. The amplitude of the disturbances were different in different stage of TC intensity evolution. Because of out-of-phase changes of kinetic energy vertically, the negligible disturbances of kinetic energy change after vertical integration during the TC transition were caused by the offset of out-of-phase changes between upper and lower levels in high-frequency disturbances of kinetic energy change, and the kinetic energy change in the upper troposphere was most notable during the TC transition, thus, the vertically integrated kinetic energy budget in the air column could not give a reasonable physical image for TC kinetic energy variation. The high-frequency disturbances might be related to convection.

Notable correlations existed among different budget terms of kinetic energy equation. Before and after the transition of Yagi, the horizontal and vertical fluxes of kinetic energy played the same role in changing the kinetic energy, and the horizontal flux of kinetic energy caused by the change of environment was related to the transition of Yagi, which was consistent with the change of kinetic energy. The correlation between the generation of kinetic energy and the horizontal flux of kinetic energy without consideration of the TC movement was rather complex. Below 500 hPa, there was a positive correlation between them, so both played the same role in changing the kinetic energy. Above 500 hPa, there was a negative correlation between them, and negative work was done by pressure gradient force to convert the kinetic energy from horizontal flux of the high-level jet stream to potential energy. Furthermore, there was negative correlation between the residual term and the vertical flux of kinetic energy. It further illustrates that the residual term was closely related to vertical convection, and played a role of inhibiting the effect caused by horizontal and vertical fluxes of kinetic energy.

Acknowledgments This work is supported by the National Natural Science Foundation of China under Grant Nos. 40830958 and 41175090.

References

Betts AK (1986) A new convective adjustment scheme. Part I: observational and theoretical basis. Q J R Meteorol Soc 112:677–691

Betts AK, Miller MJ (1986) A new convective adjustment scheme. Part II: single column tests using GATE wave, BOMEX, ATEX and arctic air-mass data sets. Q J R Meteorol Soc 112:693–709

Bosart LF, Lackmann GM (1995) Postlandfall tropical cyclone reintensification in a weakly baroclinic environment: a case study of hurricane David (September 1979). Mon Weather Rev 123:3268–3291

Chen TC, Alpert JC, Schlatter TW (1978) The effects of divergent and nondivergent winds on the kinetic energy budget of a mid-latitude cyclone: a case study. Mon Weather Rev 106:458–468

Chien HH, Smith LF (1977) Synoptic and kinetic energy analysis of hurricane Camille (1969) during transit across the southeastern United States. Mon Weather Rev 105:67–77

DiMego GJ, Bosart LF (1982) The transformation of tropical storm Agnes into an extratropical cyclone. Part II: moisture, vorticity and kinetic energy budgets. Mon Weather Rev 110:412–433

Dudhia J (1989) Numerical study of convection observed during the winter monsoon experiment using a mesoscale two-dimensional model. J Atmos Sci 46:3077–3107

Evans JL, Hart RE (2003) Objective indicators of the life cycle evolution of extratropical transition for Atlantic tropical cyclone. Mon Weather Rev 131:909–925

Haimberger L (1998) Estimating the conversion rate in the kinetic energy of sub-gridscale motions. Phys Chem Earth 23:623–628

Harr PA, Elsberry RL (2000) Extratropical transition of tropical cyclones over the western North Pacific. Part I: evolution of structural characteristics during the transition process. Mon Weather Rev 128:2613–2633

Harr PA, Elsberry RL, Hogan TF (2000) Extratropical transition of tropical cyclones over the western North Pacific. Part II: the impact of midlatitude circulation characteristics. Mon Weather Rev 128:2634–2653

Hart RE (2003) A cyclone phase space derived from thermal wind and thermal asymmetry. Mon Weather Rev 131:585–616

Hong S-Y, Dudhia J, Chen S-H (2004) A revised approach to ice microphysical processes for the bulk parameterization of clouds and precipitation. Mon Weather Rev 132:103–120

Hong S-Y, Noh Y, Dudhia J (2006) A new vertical diffusion package with an explicit treatment of entrainment processes. Mon Weather Rev 134:2318–2341

Janjic ZI (1994) The step-mountain eta coordinate model: further developments of the convection, viscous sublayer and turbulence closure schemes. Mon Weather Rev 122:927–945

Janjic ZI (2000) Comments on "Development and Evaluation of a Convection Scheme for Use in Climate Models". J Atmos Sci 57:3686

Jones SC et al (2003) The extratropical transition of tropical cyclones: forecast challenges, current understanding, and future directions. Weather Forecast 18:1052–1092

Klein PM, Harr PA, Elsberry RL (2000) Extratropical transition of western North Pacific tropical cyclones: an overview and conceptual model of the transformation stage. Weather Forecast 15:373–395

Kornegay FC, Viecent DG (1976) Kinetic energy budget analysis during interaction of tropical storm Candy (1968) with an extratropical frontal system. Mon Weather Rev 104:849–859

Kung EC (1966) Kinetic energy generation and dissipation in the large-scale atmospheric circulation. Mon Weather Rev 94:67–82

Lin Y-L, Farley RD, Orville HD (1983) Bulk parameterization of the snow field in a cloud model. J Climate Appl Meteor 22:1065–1092

Mlawer EJ, Taubman SJ, Brown PD, Iacono MJ, Clough SA (1997) Radiative transfer for inhomogeneous atmosphere: RRTM, a validated correlated-k model for the longwave. J Geophys Res 102(D14):16663–16682

Moeng C-H, McWilliams JC, Rotunno R, Sullivan PP, Weil J (2004) Investigating 2D modeling of atmospheric convection in the PBL. J Atmos Sci 61:889–903

Petterssen S, Smebye SJ (1971) On the development of extratropical cyclones. Q J R Meteorol Soc 97:457–482

Sinclair MR (1993) Synoptic-scale diagnosis of the extratropical transition of a Southwest Pacific tropical cyclone. Mon Weather Rev 121:941–960

Skamarock WC, Klemp JB, Dudhia J, Gill DO, Barker DM, Duda MG, Huang XY, Wang W, Powers JG. 2008. A description of the Advanced Research WRF Version 3. NCAR/TN-475+STR. [Available at http://www.mmm.ucar.edu/wrf/users/docs/arwv3.pdf.]

Song J, Han J, Wang Y (2011) Cyclone phase space characteristics of the extra-tropical transitioning tropical cyclones over western North Pacific. Acta Meteorol Sin 25:78–90

Wahab MA, Basset HA (2000) The effect of moisture on the kinetic energy budget of a Mediterranean cyclone. Theor Appl Climatol 65:17–36

Wang Y (2001) An explicit simulation of tropical cyclones with a triply nested movable mesh primitive equation model: TCM3. PartI: model description and control experiment. Mon Weather Rev 129:1370–1394

Zhong Z, Zhang J (2006) Explicit simulation on the track and intensity of tropical cyclone Winnie (1997). J Hydrodyn 18:641–652